Received: 13 December 2018 | Revised: 11 June 2019 | Accepted: 19 July 2019

DOI: 10.1002/navi.333

ORIGINAL ARTICLE

WILEY ION

GNSS yaw attitude estimation: Results for the Japanese Quasi-Zenith Satellite System Block-II satellites using single- or triple-frequency signals from two antennas

André Hauschild

German Aerospace Center (DLR), German Space Operations Center (GSOC), Weßling, Germany

Correspondence
André Hauschild, German Aerospace Center (DLR), German Space Operations Center (GSOC), Weßling, Germany.
Email: andre.hauschild@dlr.de

Abstract

The Japanese Quasi-Zenith Satellite System (QZSS) constellation has added three new Block-II satellites, which broadcast ranging signals from their main L-band antenna together with augmentation signals from separate, auxiliary antennas. After determination of the baseline vector between main and auxiliary antenna, differential processing allows for an estimation of the satellite's yaw attitude with an accuracy of less than 1°. Differential carrier-phase center variation maps have been derived. Yaw estimation results are presented for periods of special interest, for example 360° yaw rotations, orbit correction maneuvers and the satellite's eclipse period, where a special pseudo-yaw steering attitude mode is applied. The second part of the paper introduces a new concept using triple-frequency signals from two different antennas for attitude determination. This method is demonstrated with QZSS measurements but is also applicable to other satellite navigation system, like the enhanced GLONASS-M satellites with L3 signal capabilities.

1 | INTRODUCTION

The Japanese Quasi-Zenith Satellite System (QZSS) is a regional navigation and augmentation constellation for the Asia-Pacific region with a focus on Japan. The satellites of QZSS transmit GPS-compatible navigation signals. Due to their eccentric and inclined orbits, the satellites reside over Japan at high elevation angles over long periods of time and thus improve the satellite visibility in urban canyons. In addition, the satellites also transmit augmentation information to enable improved navigation accuracy for pseudorange-based and carrier-phase-based positioning and provide integrity information.[1,2]

The constellation of four spacecraft has recently been completed with the launch of three additional satellites. QZS-2 and QZS-4 were launched in August and November 2017 into inclined geosynchronous (IGSO) orbits. QZS-3 was launched in October 2017 into a geostationary orbit. The three new satellites are referred to as Block-II and differ from their predecessor, the Block-I satellite QZS-1, with respect to the spacecraft bus design, the signal transmitting capabilities, and the attitude control. After being set healthy, the three new satellites have provided trial services[3] and as well as the official QZSS service (together with QZS-1) since November 1, 2018.

A common feature of all four QZSS satellites is the presence of one or more additional antennas, which are used for the transmission of additional augmentation signals. All four satellites are equipped with a separate antenna for the sub-meter level augmentation service (SLAS) signal

on the L1 frequency. Only the Block-II satellite generation has a second separate antenna for the transmission of the position technology verification service (PTV) signal on the L5 frequency. The configurations for the three different satellite models are depicted in Figure 1. It becomes obvious that the relative positions for the main L-band and the SLAS and PTV antennas are different for each satellite type. It is also interesting to note that the geostationary satellite is equipped with a patch antenna array compared to the helix arrays used on the other spacecraft.

The presence of a second antenna allows for directly determining the satellite's yaw attitude if the baseline vector between the two antennas is known. By processing differences of the SLAS or PTV signal and a signal from the main L-band antenna, which share the same frequency, all errors and delays due to satellite orbit and clock as well as atmospheric effects can be canceled. This method has been demonstrated using observations from a network of geodetic receivers in the Asia-Pacific region.[5]

Being able to independently determine a GNSS satellite's yaw attitude is an interesting feature in case the actual orientation deviates from the nominal one. In the case of QZS-1, the satellite's attitude mode is changed from yaw steering to orbit normal mode. In yaw steering mode, the satellite is continuously reoriented around the nadir axis such that the solar panels face the Sun and maximal power output is ensured. This attitude mode is typically used by navigation satellites in medium Earth orbit (MEO).[6,7] In orbit normal mode, the satellite is kept fixed with respect to the orbital frame, which results in a constant yaw angle. This attitude mode is typically used by GEO satellites, like QZS-3, or temporarily also by GNSS satellites, when orbit correction maneuvers are performed. This switch of the attitude mode happens four times per year, when the Sun's elevation angle with respect to the orbit plane β is close to 20°.[4] An analysis of yaw angle estimation results for QZS-1 over the entire time of operation has shown that the transitions between the two attitude modes do not always happen exactly at the 20° threshold. Instead, the switch can be delayed by several hours.[5]

Contrary to their predecessor, the new QZSS Block-II IGSO satellites do not switch to orbit normal mode and are constantly operated in yaw steering mode. This poses the challenge, that for small angles of β, the required yaw angle rate to keep the sun-pointing mode exceeds the maximal rate with which the satellite can be rotated. In the most extreme case, for β=0, the satellite would have to rotate instantly by 180°. In reality, this problem is solved by starting the yaw rotation ahead of time such that the satellite first leads and then lags required orientation.[8] An example for a midnight turn of QZS-2, when β is approximately 0.1°, is shown in Figure 2. The black curve in the top plot depicts the nominal yaw attitude model, and the red curve is the yaw angle according to the pseudo-yaw steering model. It can be seen that the satellite's true yaw orientation deviates from the assumed nominal orientation by more than 70°.

Incorrect assumptions on a GNSS satellite's yaw orientation introduce errors in the positioning solution due to the impact of satellite attitude on modeling the solar radiation pressure, satellite antenna offset, and carrier-phase wind-up effects. Also, precise orbit determination solutions of the satellite itself are affected for the same reason. In the case of QZSS, the main L-band antenna offset in the x- and y-directions is small, and thus, the resulting error is negligible, but solar radiation pressure and phase wind-up modeling will still be affected.

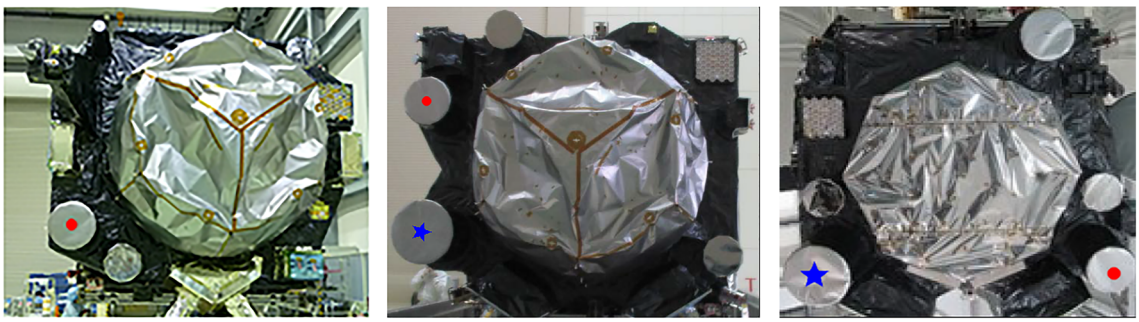

FIGURE 1 QZS-1 (left), QZS-2/-4 (middle), and QZS-3 (right) satellite antenna configurations (imagery courtesy: JAXA). The main L1/L2/L5 antenna is visible in the center of the satellites' NADIR panel and is surrounded by smaller auxiliary antennas. The red dot indicates the L1 SLAS antenna, and the blue star indicates the L5 PTV antenna. All three pictures are oriented such that the body-fixed x-axis points to the right and the y-axis points upwards, which is consistent with the attitude convention of the International GNSS Service (IGS) and rotated by 180° about the z-axis with respect to the manufacturer conventions[4] [Color figure can be viewed at wileyonlinelibrary.com and www.ion.org]

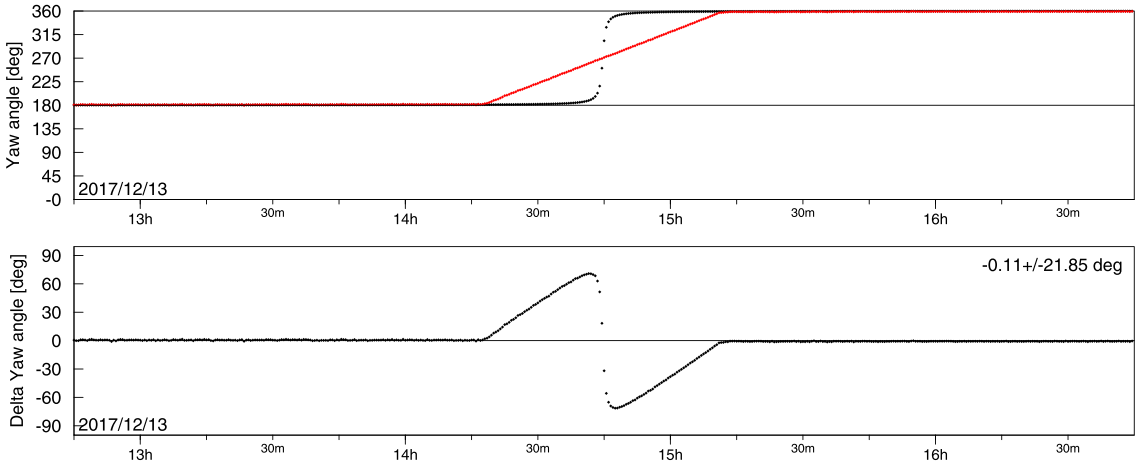

FIGURE 2 Example for a midnight turn of QZS-2 with yaw rate limitation. Yaw angles for pseudo-yaw steering (red) and nominal yaw steering (black) are shown in the top plot. The deviation of both attitude models is shown in the bottom plot. The maximum yaw angle rate at 14:45 h is approximately 1.5° /s [Color figure can be viewed at wileyonlinelibrary.com and www.ion.org]

2 | L1/L5 SLAS-BASED YAW ATTITUDE FOR QZSS BLOCK-II SATELLITES

The first part of this paper introduces yaw attitude estimation results using pseudorange and carrier-phase differences of the L1 SLAS or L5 PTV observations and L1 or L5 ranging observations. All QZSS satellites broadcast the SLAS/PTV signals from separate antennas with significant offset to the main L-band antenna used for the ranging signals. Differential processing of SLAS/PTV and ranging signals on the same frequencies eliminates all common errors like satellite orbit errors, receiver, and satellite clock offsets, as well as delays caused by troposphere and ionosphere. The only remaining terms in the differential measurements are the differential code biases for the pseudorange observations, the differential ambiguities for the carrier-phase observations, and finally, the projection of the antenna baseline vector on the line-of-sight vector. The last term depends on the satellites' attitude. Thus, if the attitude is assumed to be known, the baseline vector can be estimated, or if the baseline vector is known, the actual yaw orientation of the spacecraft is observable.

The typical approach is to first estimate a constant baseline vector in the satellite's body-fixed coordinate frame using data for which the satellite attitude is well known. Time periods with non-nominal attitude orientation, for example, during orbit maneuvers or tests, are excluded. Then, using the baseline vector results as fixed parameters and instead estimating the yaw angle, the attitude of the satellite can then be determined at all time periods, including phases with non-nominal orientation. In addition to either the three constant baseline vector coordinates or the epoch-dependent yaw angle, the algorithm also estimates single differences of carrier-phase ambiguities and code biases between two signals. Differences of pseudorange and carrier-phase observations between L1 SLAS and L1 C/A-code or the L5 PTV and the L5 ranging signal are processed. Details of the estimation algorithms can be found in Hauschild et al.[5]

An additional refinement to the previously published results is the calibration of differential antenna phase-center variations between the SLAS antenna and the main L-band antenna. It will be shown that these variations are a significant error source for yaw angle estimation. The calibration procedure and results for the differential phase-center maps and the baseline vectors are presented in the next section. The subsequent section will then present selected yaw attitude determination results using the differential phase-center variation corrections.

2.1 | Baseline estimation and differential phase-center variations

The calibration and antenna baseline determination is done in an iterative process, where the yaw attitude of the QZSS satellite is assumed to be known, and only the three coordinates of the baseline vector, differential pseudorange biases, and differential carrier-phase ambiguities are estimated. Data of approximately 12 months between August 2017 and September 2018 has been used for the estimation of the baselines.[9,10]

Table 1 shows the results for the estimated baseline vector of the L1 SLAS antenna for QZS-1 (Block-I) and the L1 SLAS and L5 PTV antennas for QZS-2/4 (Block-II). Note that a baseline estimation for the geostationary satellite QZS-3 could not be done due to the limited tracking coverage of the geodetic reference station network. It

TABLE 1 Estimates of baseline vector components and corresponding standard deviation between the L1 SLAS and L5 PTV antenna and the main L-band antenna for Block-I satellite QZS-1 (PRN J01) and Block-II satellites QZS-2/-4 (PRN J02/J03). QZS-1 is not equipped with an L5 PTV antenna. The baseline vectors point from the main L-band antenna to the corresponding SLAS/PTV antenna

	QZS-1 (J01)			QZS-2/-4 (J02/J03)		
Antenna	**x (m)**	**y (m)**	**z (m)**	**x (m)**	**y (m)**	**z (m)**
L1 SLAS	−1.1482	−0.6922	+0.1522	−1.2587	+0.4196	+1.3301
	(±0.0012	±0.0020	±0.0184)	(±0.0027	±0.0046	±0.0266)
L5 PTV	–	–	–	−1.2600	−0.5710	−0.0771
				(±0.0026	±0.0022	±0.0465)

should also be noted that for the estimation of the L5 PTV antenna offset, measurements from only up to five tracking stations were available, compared to 20 to 30 stations for the L1 SLAS baseline.

The results for the differential carrier-phase variation maps for the L1 SLAS antenna are shown in Figure 3. The left plot depicts the results for the Block-I satellite QZS-1 and the right plot shows the map for the Block-II satellite QZS-2. It becomes obvious that for both satellites, the antenna pairs are affected by differential phase variations of a few millimeters peak-to-peak. It can also be seen that the pattern of QZS-2 is more pronounced and looks dissimilar to the pattern of QZS-1, which indicates that individual calibrations are required for both satellites types.

The effect of the phase-center variation calibration on the attitude solution is depicted in Figure 4. Both plots show yaw angle errors between the modeled nominal yaw steering attitude of QZS-2 on January 5, 2018 without (top plot) and with (bottom plot) phase-center calibration maps applied. It becomes obvious that the application of the corrections reduces the bias in the yaw angle by more than 50% from 0.37° to 0.16° and the standard deviation by 35% from 0.60° to 0.39 °.

2.2 | Single-frequency yaw-determination results

With the baseline vectors and phase-center variation corrections available, the yaw orientation of the QZSS satellites can now be determined. The following sections show selected examples of interesting yaw angle orientations of the two QZS Block-II spacecraft QZS-2 and QZS-4. Note that the attitude determination results have been computed using SLAS and C/A-code ranging observations on the L1 frequency only. In principle, the observations of the PTV and the ranging signal on L5 could be used as well, but few receivers currently support tracking of these signals. The RINEX format update to version 3.04,

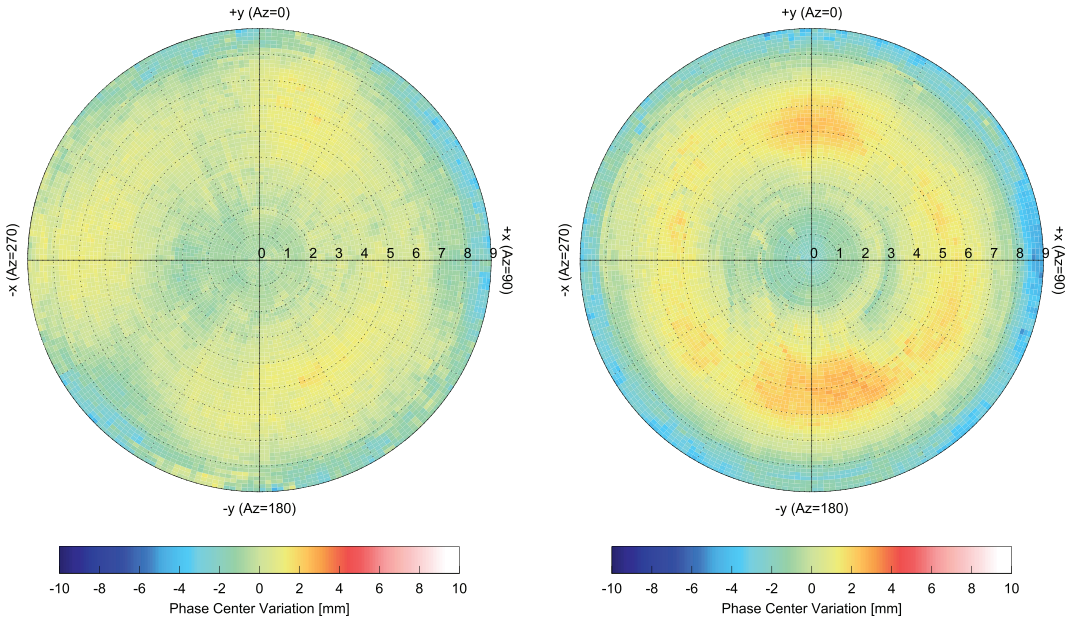

FIGURE 3 Map of differential phase-center variations for QZS-1 (PRN J01) (left plot) and QZS-2 (PRN J02) (right plot) between SLAS antenna and main L-band antenna for L1 SLAS. The plot range is limited to a maximum off-boresight angle of 9° [Color figure can be viewed at wileyonlinelibrary.com and www.ion.org]

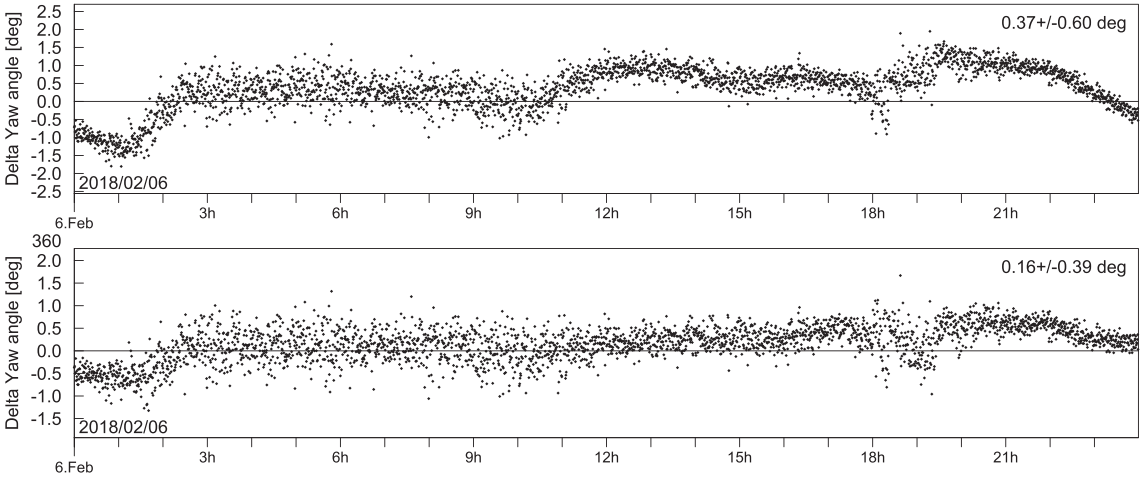

FIGURE 4 Yaw angle estimation errors for QZS-2 on January 5, 2018, without (top plot) and with (bottom plot) corrections for phase-center variations applied. The satellite is in nominal yaw steering mode

which officially supports the L5 PTV observations, was only released in December 2018. Thus, at the time of writing, receivers did not yet support this standard.

2.3 | 360° yaw turns

The plots in Figure 5 show how QZS-2 performs 360° yaw rotations. The top plot shows a single rotation over a time interval of approximately 2 hours, which corresponds to a yaw rate of about 0.05°. This maneuver was performed on December 2, 2017, at $\beta \approx 8°$, before the satellite entered the eclipse period four days later for the first time since it was launched. The turn was presumably a test to see if the satellite was able to rotate at the yaw rate limit of 0.055°, which it would do during a noon turn or midnight turn. A similar maneuver was observed on January 1, 2018, after the end of the eclipse period. Interestingly, QZS-2 was rotated four times around the z-axis in the reverse direction over a time interval of approximately 8 hours at a β-angle of −13°.

2.4 | Pseudo-yaw steering mode in eclipse phase

As already mentioned, the QZS Block-II satellites QZS-2 and QZS-4 do not switch to orbit normal mode like their predecessor QZS-1, but instead perform a so-called pseudo-yaw steering when the required yaw rate for nominal yaw steering exceeds a threshold value of ±0.055°/s. This can happen when the β-angle is between −5° and +5°.[8] For QZS-2, the first period with pseudo-yaw steering started on December 6 and ended on December 21, 2017. The longest orbit noon and midnight turns

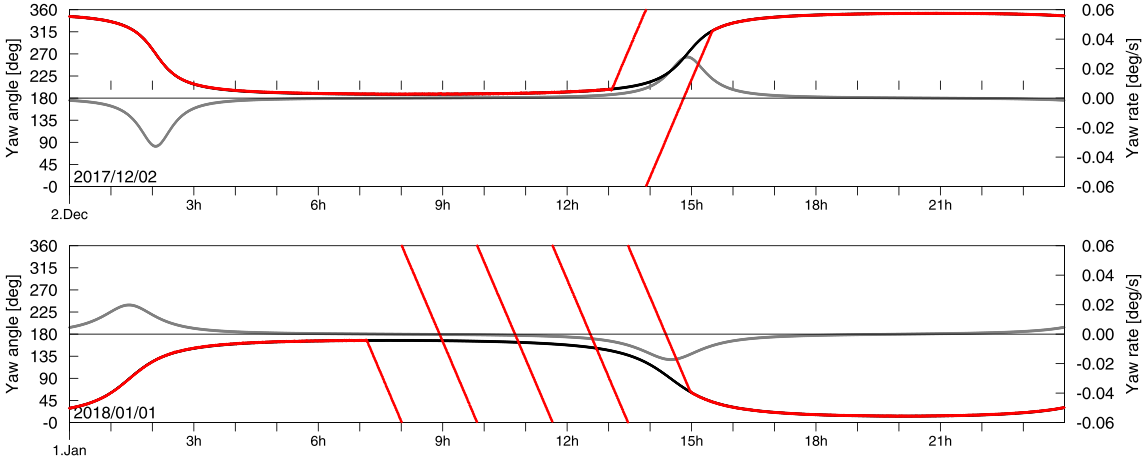

FIGURE 5 QZS-2 performing 360° yaw rotations on December 2, 2017 (top plot), and January 1, 2018 (bottom plot). Modeled (black) and estimated (red) yaw attitude shown together with the nominal yaw rate (gray) [Color figure can be viewed at wileyonlinelibrary.com and www.ion.org]

happened on December 13, when β was close to zero. QZS-4 was in a pseudo-yaw steering period from April 20 until May 19, 2018. The longest noon and midnight turns happened on May 4.

The plot in Figure 6 depicts the estimated and modeled yaw angle results together with the nominal yaw rate in the upper plot for December 13. It becomes obvious that during the noon and midnight turn periods, the nominal yaw rate exceeds the threshold and the satellite performs a rotation with the limited yaw rate. The bottom plot in Figure 6 depicts the differences between the estimated yaw angle and the modeled yaw angle as described in a previous article.[8] The results show that the orientation can be estimated with an accuracy on the order of a few degrees. No significant offsets are visible during the noon or midnight turn, which means that the pseudo-yaw steering mode can actually be modeled with sufficient accuracy. The plot in Figure 7 shows the noon and midnight turns for QZS-4 on May 4, 2018.

It is interesting to note in this context that the direction of the rotation cannot be predicted in the case when $|\beta|<0.03°$ due to measurement uncertainties onboard the spacecraft,[8] which would lead to a maximum yaw angle error of 180° between the true and modeled attitude. However, this problem can only occur twice a year, if a noon or midnight turn coincides with a very small β-angle. For the first eclipse periods of QZS-2 and QZS-4, such an event could not be observed.

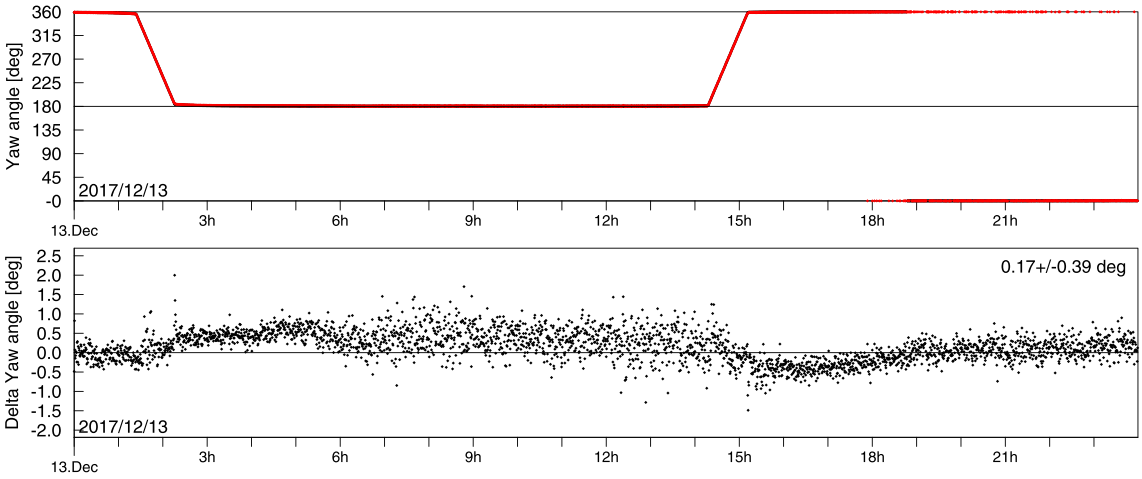

FIGURE 6 QZS-2 performing noon and midnight turns on December 13, 2017, with yaw rate limitation. The estimated yaw angle is plotted in red in the top plot. The deviations from modeled yaw angle is shown in black in the bottom plot. The maximum, nominal yaw angle rate at 14:45 h is approximately 1.5°/s [Color figure can be viewed at wileyonlinelibrary.com and www.ion.org]

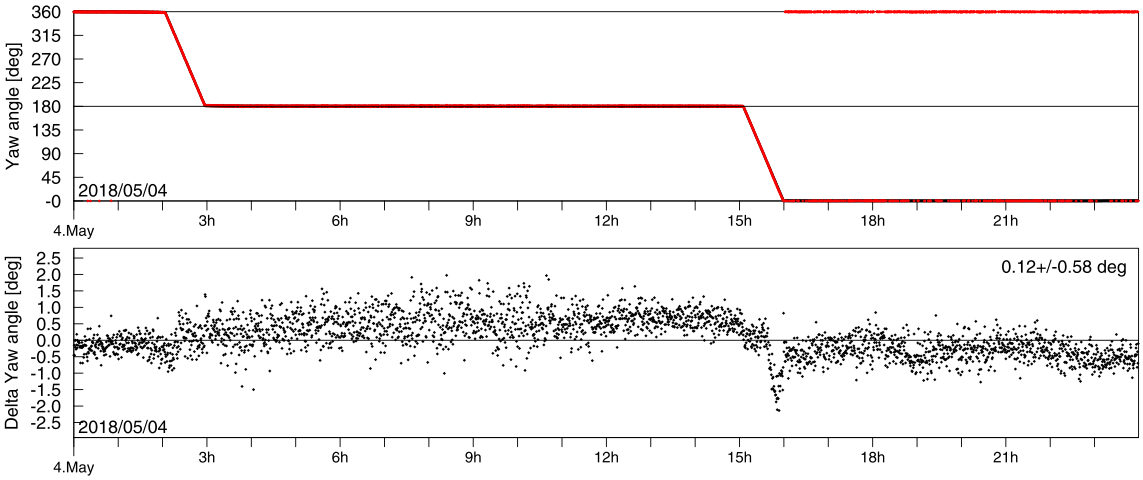

FIGURE 7 QZS-4 performing noon and midnight turns on May 5, 2018, with yaw rate limitation. The estimated yaw angle is plotted in red in the top plot. The deviations from modeled yaw angle are shown in black in the bottom plot. The maximum, nominal yaw angle rate at 15:30 h is approximately −3.5°/s [Color figure can be viewed at wileyonlinelibrary.com and www.ion.org]

2.5 | Orbit normal mode

Another interesting case during which the true orientation the QZSS satellites deviates from the modeled orientation is orbit maneuvers. The spacecraft is reoriented into orbit normal mode for the duration of the maneuver to point the thrusters of the orbit control system into the proper directions. In this orientation, the satellite's body-fixed axes are aligned with the orbital frame axes. In this case, the satellite's body-fixed *x*-axis (according to IGS conventions) points in the anti-flight direction, which corresponds to a yaw angle of 180°.

An example orbit maneuver for QZS-2 is shown in Figure 8. The satellite is in nominal yaw steering mode until approximately 7:00 h UTC, when it is reoriented to orbit normal mode. It remains in this orientation until approximately 19:00 h UTC, when it is reoriented back into yaw steering mode. It is interesting to note that the yaw angle rate during the reorientation from orbit normal mode to yaw steering mode is on the order of 0.5°/s and thus about a factor of 10 larger than the yaw rate during orbit noon or midnight turns. It should also be noted that the maneuver on January 6 has been announced (NAQU 2017141) and the satellite was set unhealthy from January 6 05:59 h UTC until January 7 03:21 h UTC.

3 | TRIPLE-FREQUENCY YAW ATTITUDE ESTIMATION

The previous results have been obtained based on differential processing of two signals on the same frequency from different antennas. As an alternative approach, it is also possible to use triple-frequency signal combinations with signals on three frequencies, of which one is transmitted from a second antenna. The basic idea is to use the three signals to form an ionosphere-free combination, still containing the geometric information resulting from the two antennas for the attitude estimation.

QZSS offers two different signal combinations, which can be used for this purpose. The first one is the combination of the L1 signals from the SLAS antenna and the L2C and L5 combination from the main L-band antenna. The second option for QZSS Block-II is to use the new L5 PTV signal from the corresponding antenna, and L1 and L2C signals from the main antenna. The following sections will first derive the triple-frequency combination observation equations and then present results for the L1-SLAS, L2C, and L5 signals. The other combination could not be used due to the limited availability of observations.

3.1 | Derivation of tripe-frequency combination

The triple-frequency combination for the attitude determination is essentially a difference of two ionosphere-free signals combinations. We start the derivation with a simplified equation for the carrier-phase observable Φ_i at frequency f_i:

$$\Phi_i = \rho_i + c(\delta t_r - \delta t^s) - I_i + T + \lambda_i(\omega + A_i) + \epsilon_i, \quad (1)$$

where ρ_i is the geometric distance from the receiver antenna to the satellite antenna, c is the speed of light, δ_r and δ^s are the receiver and satellite clock offsets, I_i is the ionospheric delay, T is the tropospheric delay, λ_i is the wavelength, ω is the carrier-phase wind-up, A_i is the carrier-phase ambiguity including the fractional carrier-phase biases, and ϵ is the observation noise. The subscript i denotes the corresponding frequency. Note that the geometric range is also frequency dependent here and can further be expanded into

$$\rho_i = ||\mathbf{r}^s + \mathbf{b}_i^s - \mathbf{r}_r||, \quad (2)$$

where $\mathbf{r}^s$ is the position vector of the satellite center of mass, $\mathbf{b}_i^s$ is the antenna offset vector from the satellite center of mass to the antenna broadcasting the signal on frequency i, and $\mathbf{r}_r$ is the receiver antenna position vector. Assuming that three carrier-phase observations Φ_1, Φ_2, and Φ_5 are available on the the corresponding frequencies f_1, f_2, and f_5, the following combined observation Φ_{125} can be formed as the difference of two ionosphere-free combinations[11-13]:

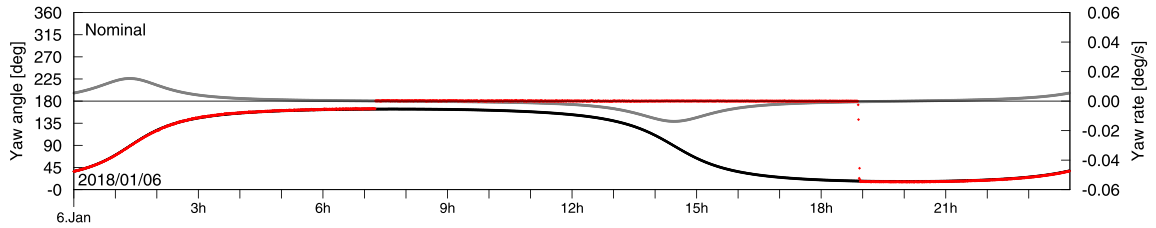

FIGURE 8 Orbit normal attitude mode for QZS-2 on January 6, 2018, between 07:00h and 19:00h UTC. Modeled (black) and estimated (red) yaw attitude shown together with the nominal yaw rate (gray) [Color figure can be viewed at wileyonlinelibrary.com and www.ion.org]

$$\begin{aligned}\Phi_{125} &= \left(\frac{f_1^2}{f_1^2-f_2^2}\Phi_1-\frac{f_2^2}{f_1^2-f_2^2}\Phi_2\right)\\ &\quad-\left(\frac{f_1^2}{f_1^2-f_5^2}\Phi_1-\frac{f_5^2}{f_1^2-f_5^2}\Phi_5\right)\end{aligned} \tag{3}$$

$$\begin{aligned}&= \left(\frac{f_1^2}{f_1^2-f_2^2}-\frac{f_1^2}{f_1^2-f_5^2}\right)\Phi_1-\left(\frac{f_2^2}{f_1^2-f_2^2}\right)\\ &\quad\Phi_2+\left(\frac{f_5^2}{f_1^2-f_5^2}\right)\Phi_5\end{aligned} \tag{4}$$

or in short, using the combination coefficients k_1, k_2, and k_5:

$$\Phi_{125} = k_1\Phi_1 + k_2\Phi_2 + k_5\Phi_5. \tag{5}$$

It becomes obvious from Equation 4 that the combination is ionosphere-free ($\sum_i k_i/f_i^2 = 0$) and geometry-free ($\sum_i k_i = 0$). When Equation 1 is substituted into Equation 5, all frequency independent terms and the ionospheric delay drop out:

$$\begin{aligned}\Phi_{125} &= k_1\rho_1 + k_2\rho_2 + k_5\rho_5\\ &\quad+(k_1\lambda_1 + k_2\lambda_2 + k_5\lambda_5)\omega\\ &\quad+k_1\lambda_1 A_1 + k_2\lambda_2 A_2 + k_5\lambda_5 A_5\\ &\quad+(k_1\epsilon_1 + k_2\epsilon_2 + k_5\epsilon_5).\end{aligned} \tag{6}$$

The only terms left in the equation are the geometric range, the carrier-phase wind-up, the ambiguities, and the measurement noise. Substitution of Equation 2 into Equation 6 introduces the the antenna offset vectors $\mathbf{b}_i$. Treating $\mathbf{b}_1$ as an unknown parameter, a first order Taylor series expansion of the equation around $\mathbf{b}_2$ leads to

$$\Phi_{125} = k_1\mathbf{e}^T\mathbf{b_{21}} + \sum_i k_i\lambda_i\omega + A_{125} + \epsilon_{125}, \tag{7}$$

where $\mathbf{e}$ is the line-of-sight vector from the receiver antenna to the main L-band antenna, $\mathbf{b_{21}}$ is the baseline vector between the SLAS and the L-band main antenna, A_{125} is a combined carrier-phase ambiguity, and ϵ_{125} is the combined observation noise. The expression has further been simplified by exploiting the knowledge that $\mathbf{b}_2{=}\mathbf{b}_5$ and the baseline vector is defined as $\mathbf{b_{21}}{=}\mathbf{b_1}{-}\mathbf{b_2}$. Assuming that the carrier-phase noise has a Gaussian distribution with the same standard deviation σ on all three frequencies, the standard deviation of the combined observation noise ϵ_{125} can be found from

$$\sigma_{125} = \sigma\sqrt{k_1^2 + k_2^2 + k_5^2}. \tag{8}$$

Values for the combination factors for the QZSS frequencies L1, L2, and L5 are provided in Table 2. The table also shows the combined carrier-phase wind-up wavelength, which amounts to only approximately 2 mm, thus the corresponding term in Equation 7 can safely be omitted. The noise amplification factor for the combined observation noise in Equation 8 is about 2.015 for the chosen coefficients. With three combination factors and only two constraint equations (ionosphere-free and geometry-free), the coefficient values in Table 2 are not the only possible choice. As a matter of fact, one coefficient can be freely chosen and the other two are linearly dependent. This is derived in detail in Appendix A.

Finally, two rotation matrices are introduced: the first one is the rotation matrix $\mathbf{R}$, which depends on the yaw angle Ψ and describes the rotation from the satellite's body-fixed coordinate system, in which the baseline vector $\mathbf{b_{21}}$ is known, into the orbital frame around the satellite's z-axis. The second is the matrix $\mathbf{O}$, which describes the rotation from the orbital frame into the Earth-centered Earth-fixed frame, in which the line-of-sight vector is given:

$$\Phi_{125} = k_1\mathbf{e}^T\mathbf{O}\mathbf{R}(\Psi)\mathbf{b_{21}} + A_{125} + \epsilon_{125}. \tag{9}$$

The two unknown parameters in this equation are the yaw angle Ψ and the combined ambiguity A_{125}. It becomes obvious that the observability of the yaw angle depends on the projection of the baseline vector on the line-of-sight vector. Thus, the best observability is provided by stations tracking the satellite at low elevation angles. It also becomes obvious that the combination factor k_1 has an effect on the estimation. For the selected signal combination, the factor k_1 is unfortunately the smallest of the three. This means that the information content of the combined observation is attenuated compared to the noise, which is amplified by a factor of 2 compared to the noise of the individual observations. The derivation in Appendix A proves that two of the coefficients are linearly dependent on the third one and that the ratio between k_1 and the noise amplification factor is always constant. Thus, this ratio cannot be improved by changing the coefficients. If instead the L5 PTV observations could be selected, the factor k_5 would give a more favorable ratio.

Of course a similar equation to Equation 9 can also be derived for the pseudorange observations. It would look identical to the carrier-phase combination, except for that the phase wind-up term is not present and the ambiguity

TABLE 2 Triple-frequency combination factors, carrier-phase wind-up wavelength, and noise amplification factor for QZSS L1, L2, and L5 signals

Factor	k_1	k_2	k_5	$\sum_i k_i\lambda_i$	$\sqrt{\sum_i k_i^2}$
Value	+0.285	−1.546	+1.261	−0.199 cm	2.015

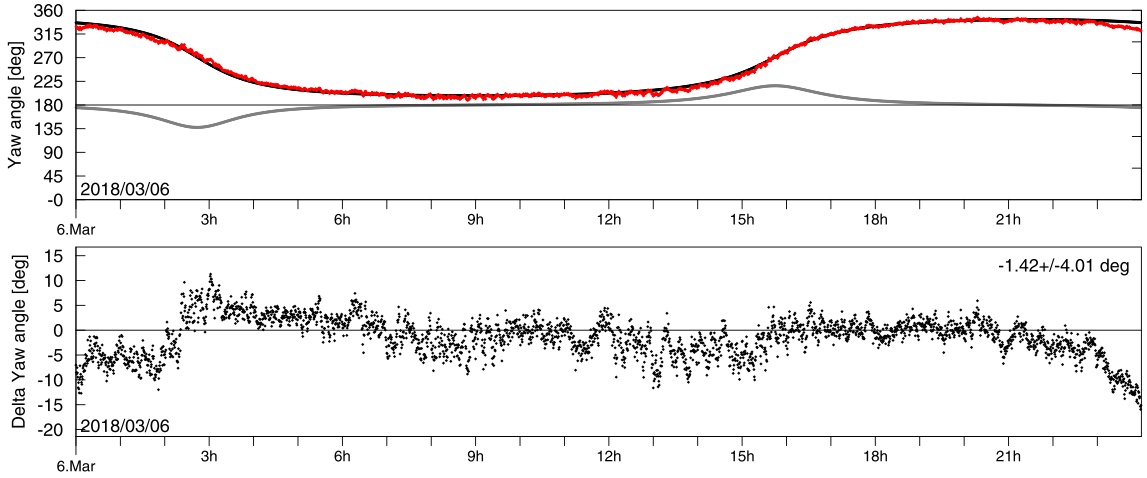

FIGURE 9 QZS-4 triple-frequency attitude determination results (top) and deviations from nominal yaw angle (bottom). Nominal (black) and estimated (red) yaw attitude shown together with the nominal yaw rate (gray) [Color figure can be viewed at wileyonlinelibrary.com and www.ion.org]

term would be a combination of the single-frequency code biases instead.

3.2 | Triple-frequency yaw-determination results

The plot in Figure 9 depicts yaw attitude determination results for QZS-4 using the ionosphere-free triple-frequency signal combination of the L1 SLAS, L2C, and L5 signals in Equation 9. The bottom plot shows the deviations of the estimated yaw angle and the nominal value. The standard deviation is approximately 4°, which is larger compared to the single-frequency attitude determination. Several reasons can be held responsible for the degraded performance. First, as already mentioned in the previous section, the unfavorable ratio of combination factors attenuates the information content in the observation equation compared to the noise. Furthermore, the three different signals in the combination are affected by different multipath errors due their different wavelength. This was not the case for the single-frequency attitude determination, since the multipath errors would cancel out in the single difference. This effect is especially pronounced for measurement at low elevation angles. Furthermore, a differential phase-center variation correction has not been applied to the triple-frequency measurements.

4 | CONCLUSIONS AND FUTURE WORK

The first part of the paper presented attitude determination results based on L1 SLAS and L1 C/A-code signals for the new Block-II QZSS satellites for interesting periods of time like eclipse season and orbit maneuvers. Results for the baseline vector between the antennas of the new L5 PTV signal and the L5 ranging signal have been presented, but a reliable attitude determination could not be performed with this signal. Few receivers currently support tracking of the new L5 SLAS signal. When the tracking coverage of the L5 PTV signal improves in the future, this signal can also be used.

In the second part of the paper, a new method for attitude determination with triple-frequency signals from two L-band antennas was presented using the example of QZSS. This method does not rely on two signals sharing the same frequency to cancel the ionosphere, which makes it more universally applicable to other navigation satellite systems, like the enhanced GLONASS-M satellites with L3 capabilities. These satellites transmit the L3 CDMA signals from a separate antenna together with the legacy L1 and L2 FDMA signals. Thus, a triple-frequency yaw attitude determination will be possible using observations from global receiver network.

The yaw angle attitude results for the triple-frequency processing have proven to be significantly more noisy and affected by systematic errors compared to the single-frequency results. Differential carrier-phase multipath, unfavorable combination coefficients, and the absence of a phase-center variation map can explain the reduced accuracy. Using the new L5 PTV observations would lead to a better ratio of information content to noise in the observation equation.

ORCID

André Hauschild https://orcid.org/0000-0002-0172-3492

REFERENCES

1. Iwama R, Soga H, Odagawa K, et al. Operation of sub-meter class augmentation system and demonstration experiments with Quasi-Zenith Satellite MICHIBIKI. In: *Proceedings of the 2012 International Technical Meeting of the Institute of Navigation*; Newport Beach, CA, January 2012:1295-1301.
2. Harima K, Choy S, Wakabayashi Y, Kogure S, Rizos C. Transmission of augmentation messages for precise point positioning utilizing Japanese QZSS LEX signal. In: *Proceedings of the 27th International Technical Meeting of the Satellite Division of the Institute of Navigation (ION GNSS+ 2014)*; Tampa, Florida; September 2014:2467-2477.
3. Steigenberger P, Thoelert S, Hauschild A, Montenbruck O, Langley RB. Constellation completed: QZS-3 and QZS-4 join the Quasi-Zenith Satellite System. *GPS World*. 2018;29(2):43-48.
4. Ishijima Y, Inaba N, Matsumoto A, et al. Design and development of the first Quasi-Zenith Satellite attitude and orbit control system. In: *Proceedings of the IEEE Aerospace Conference*; March 2009; Big Sky, MT:1-8.
5. Hauschild A, Steigenberger P, Rodriguez-Solano C. QZS-1 yaw attitude estimation based on measurements from the CONGO network. *NAVIGATION*. 2012;59:237-248.
6. Bar-Sever YE. A new model for GPS yaw attitude. *J Geod*. 1996;70(11):714-723.
7. Dilssner F, Springer T, Gienger G, Dow J. The GLONASS-M satellite yaw-attitude model. *Adv Space Res*. 1996;47(1):160-171.
8. Cabinet Office. QZS-2 Satellite Information (SPI-QZS2-B). Tech. rep., Government of Japan National Space Policy Secretariat; 2018.
9. International GNSS Service (IGS). Daily 30-second GNSS Observation Data. https://doi.org/10.5067/gnss/gnss_daily_o_001; 1992.
10. Johnston G, Riddell A, Hausler G. The international GNSS service. In: Teunissen PJ, Montenbruck O, eds. *Springer Handbook of Global Navigation Satellite Systems*. Cham: Springer; 2017:967-982.
11. Simsky A. Three's the charm: triple frequency combinations in future GNSS. *Inside GNSS*. 2006;1(5):38-41.
12. Montenbruck O, Hauschild A, Steigenberger P, Langley RB. Three's the challenge: a close look at GPS SVN62 triple-frequency signal combinations finds carrier-phase variations on the new L5. *GPS World*. 2010;21(8):8-18.
13. Montenbruck O, Hugentobler U, Dach R, Steigenberger P, Hauschild A. Apparent clock variations of the Block IIF-1 (SVN62) GPS satellite. *GPS Solutions*. 2012;16(3):303-313.

How to cite this article: Hauschild A. GNSS Yaw Attitude estimation: Results for the Japanese Quasi-Zenith Satellite System block-II satellites using single- or triple-frequency signals from two antennas. *NAVIGATION*. 2019;66:719–728. https://doi.org/10.1002/navi.333

APPENDIX A

The coefficients presented in Table 2 for the linear combination in Equation 5 are not the only possible choice. The following derivations will show that the coefficients can actually arbitrarily be changed without any impact on the triple-frequency attitude solution.

The triple-frequency combination is ionosphere-free and geometry-free, which leads to the following two constraints on the coefficients:

$$k_1 + k_2 + k_5 = 0, \tag{A1}$$

$$k_1/f_1^2 + k_2/f_2^2 + k_5/f_5^2 = 0. \tag{A2}$$

With three coefficients and two constraint equations, one of the coefficients can be chosen freely and the other two can be expressed as a function of the free parameter. Defining the constant $a = \frac{f_1^2 f_2^2 - f_2^2 f_5^2}{f_1^2 f_2^2 - f_1^2 f_5^2}$ and using the constraint equations (Equations A1 and A2), the following linear dependencies for the coefficients can be found:

$$k_2 = a k_1, \tag{A3}$$

$$k_5 = -(1 + a) k_1. \tag{A4}$$

Substitution of Equations A3 and A4 into the expression for the noise amplification (Equation 8) yields the following dependency on the coefficient k_1:

$$\sigma_{125} = k_1 \sqrt{2(1 + a + a^2)}. \tag{A5}$$

This derivation shows that the noise amplification factor directly depends on the selected value for the coefficient k_1. Therefore, the ratio of the k_1 and the combined noise is always constant irrespective of the choice of this coefficient. It is therefore not possible to achieve a more favorable ratio between the coefficient k_1, which affects the yaw angle estimate, and the combined noise by scaling the selected coefficients. The only feasible option is to have one of the other two signals available on the auxiliary antenna to provide larger values for the combination coefficients.